



RESEARCH PAPER

Coprecipitation Synthesis of Fe-Doped TiO₂ from Various Commercial TiO₂ for Photocatalytic Reaction

Imane Ellouzi¹ · Souad El hajjaji¹ · Mourad Harir^{2,3} · Philippe Schmitt-Kopplin^{2,3} · Larbi Laânbab⁴

Received: 14 May 2020 / Revised: 28 August 2020 / Accepted: 10 September 2020 / Published online: 26 September 2020
© University of Tehran 2020

Abstract

The current work reports the synthesis of Fe-doped TiO₂ nanoparticles by simple coprecipitation method and compares their photocatalytic efficiency to three different commercially available TiO₂ (i.e., Sachtopore, Hombikat UV100 and Fluka) using methyl orange (MO) under UV light irradiation. X-ray diffraction (XRD), diffuse reflectance spectroscopy (DRS) and transmission electron microscopy (TEM) were used to characterize these synthesized Fe-doped TiO₂ nanoparticles. In fact, the DRS results revealed that the bandgap of doped photocatalysts is smaller compared to undoped TiO₂, leading to a slight shift in the absorption band towards the beginning of the visible light. In addition, XRD has shown that all samples were well crystallized and have only anatase phase. Accordingly, the photocatalytic investigation revealed that doped TiO₂ exhibited improved photocatalytic efficiency of methyl orange (MO) compared to undoped TiO₂ photocatalysts and depends on iron constituents, TiO₂ types as well as the doses of synthesized nanomaterials.

Article Highlights

- A simple coprecipitation method for the synthesis of Fe-doped TiO₂ photocatalysts and comparison of their photocatalytic efficiency to undoped TiO₂.
- All Fe-doped TiO₂ showed smaller bandgap compared to undoped TiO₂ with only anatase phase.
- Fe-doped TiO₂ improves the photocatalytic degradation of dyes compared to undoped TiO₂.
- Photocatalytic efficiency of these doped TiO₂ depends on their doses, the constituents of iron and TiO₂ types.

Keywords Photocatalytic activity · Coprecipitation · Metal oxide · Water treatment · Azo dye

Introduction

Air and water pollution are major problems facing modern societies. About half of the global production of synthetic textile dyes (700,000 tons per year) belong to azo products, which have chromophore (–N=N–) in their molecular structures (Yan-Xia et al. 2015). Various traditional physical and chemical techniques have been studied elsewhere (Yan-Xia et al. 2015; Auta et al. 2013; Taghizadeh et al. 2013; Ferroudj et al. 2013) to treat textile wastewater such as adsorption and chemical precipitation, but they are not favorable since these methods require further treatment to eliminate hazardous wastewater. However, advanced oxidation processes (AOPs) have proved to be an effective and promising treatment method for the removal of environmental contaminants (Bilińska et al. 2017; Meek et al. 2017). Thus, it is based on the excitation of a semiconductor mainly of

✉ Imane Ellouzi
im.ellouzi@gmail.com

✉ Souad El hajjaji
souad.elhajjaji@um5.ac.ma

¹ Laboratory of Spectroscopy, Molecular Modeling, Materials, Nanomaterials, Water and Environment, CERNE2D, Faculty of Sciences, Mohammed V University in Rabat, Av. Ibn Batouta, BP 1014, Rabat, Morocco

² Research Unit Analytical BioGeoChemistry, Department of Environmental Sciences, Helmholtz Zentrum Muenchen, Ingolstaedter Landstrasse 1, 85764 Neuherberg, Germany

³ Technical University of Munich, Maximus von Imhof Forum 2, 85354 Freising-Weihenstephan, Germany

⁴ Laboratory of Conception and Systems, Faculty of Sciences, Av. Ibn Batouta, BP 1014, Rabat, Morocco

titanium dioxide TiO_2 using UV and/or visible light. Under the action of photons, this semiconductor (or photocatalyst) produces highly oxidizing free radicals. Consequently, it can oxidize a wide range of pollutants and ultimately mineralize them into CO_2 and H_2O moieties (Koupaie et al. 2013; Hejazi et al. 2020; Chatzisyneon et al. 2013; Pang et al. 2013).

Metal-oxide semiconductors are widely studied in several green applications such as photocatalytic environmental remediation, especially wastewater decontamination (Anjum et al. 2016; Srikanth et al. 2017; Zhang et al. 2017a; Gomathi Devi et al. 2014). Among the semiconductors studied, titanium dioxide (TiO_2) has attracted considerable attention in the field of photochemistry (Sun et al. 2018), due to its low cost, its non-toxic nature, long-term stability and its strong photocatalytic activity (Weng et al. 2016). TiO_2 is the most suitable semiconductor used in photocatalysis. However, its activity is limited to the UV region of the solar radiation. In fact, there are three naturally occurring TiO_2 phases: anatase, rutile, and brookite. Therefore, the anatase phase is widely considered to have higher photocatalytic activity.

Doping is one of the most widely used approaches to shift the spectral response of wide bandgap semiconductors to visible light, where certain metal ions can be used as dopants such as copper (Zhang et al. 2017b), zinc (Naira et al. 2017) and nickel (Liu et al. 2017). Among the various dopants, iron has been extensively studied because the radius of Fe^{3+} (0.64 Å) is close to that of Ti^{4+} (0.68 Å) (Zahid et al. 2018). Therefore, Fe ions can be easily incorporated into the crystal lattice of TiO_2 (Crişana et al. 2018). Doping with Fe^{3+} could introduce higher oxygen vacancies in the crystal lattice or on the surface of TiO_2 , which promote the photocatalytic activity by promoting the adsorption of water and the formation of hydroxyl groups on the surface of TiO_2 (Han et al. 2009).

Generally, semiconductors are used in a variety of applications; for the removal of chemical pollutants (Ghaedi et al. 2013), photocatalysis (Black et al. 2018) and solar cell and gas sensors; have been widely reported (Liao et al. 2016) due to their special electronic and optical properties (Yanga et al. 2012). In recent years, methyl orange has been one of the most organic pollutants studied. However, the photocatalytic degradation of methyl orange (MO) in aqueous media is always chosen as a model reaction to study the photocatalytic efficiency of photocatalysts. In this study, three commercially available TiO_2 were chosen to investigate their performances on photodegrading MO dye. Thus, several methods have been reported for the preparation of TiO_2 semiconductors such as sol-gel, hydrothermal and coprecipitation. The coprecipitation method has certain advantages/disadvantages compared to conventional processes. In fact, the main advantage of the coprecipitation process is cost-effective; the large number

of nanoparticles can be synthesized in a short time, high production yields and synthesis at room temperature (Cruz et al. 2018; Wu et al. 2016). However, this technique has several drawbacks such that the control of particle size distribution is limited (Nawaz et al. 2019). Grinding the calcined powder is sometimes required to achieve the desired particle size and contributes to reduced purity. The aim of this study is to prepare and assess the effects of the amount of Fe-doped TiO_2 and the nature of TiO_2 on the structural and optical properties of different TiO_2 nanoparticles synthesized by the coprecipitation method.

Experimental

Materials

Commercially available TiO_2 with different structures were obtained from different sources. TiO_2 Hombikat UV-100 powder (Sachtleben Chemie, Germany; Purity > 99%) is composed of pure anatase and characterized by a specific surface area (SSA) larger than 250 m^2/g (Chnirheb 2012). TiO_2 Degussa P25 (Sigma-Aldrich, Germany; Purity > 99.5%) contains more than 80% anatase and 20% of rutile and a specific surface area (SSA) larger than 50 m^2/g . TiO_2 (Fluka; Purity > 99%) has a specific surface area of 10 m^2/g and a crystal structure of 100% anatase. Ferrous sulfate (FeSO_4 , 99%), ferric chloride (FeCl_3 , 97%), HCl 37%, NaOH 97% were purchased from Sigma-Aldrich. All reagents were used without any further purification, and all stock and working solutions were prepared in deionized water.

Synthesis of Fe-Doped TiO_2

Three different sources of TiO_2 (Hombikat UV-100, Fluka, and Sachtopore) were assessed without any further treatment. Ferrous sulfate (FeSO_4), ferric chloride (FeCl_3) were used as precursors for iron. TiO_2 semiconductor nanoparticles were prepared by coprecipitation method to obtain FeSO_4 or $\text{FeCl}_3/\text{TiO}_2 = 0.1\%$ and 0.2% (wt) powders. The amount desired of iron and TiO_2 were dissolved in 30 mL of HCl (0.25 M) solution. The solution was sonicated for 2 h to ensure the homogeneity. Furthermore, NaOH (0.1 M) was added into the solution as the co-precipitant to adjust the pH value. Then the solution was filtered and the precipitate was washed with deionized water and dried at 50 °C. The obtained photocatalysts were ground with a mortar and then calcined at 500 °C for 2 h with a constant heating rate of 5 °C/min.

Characterizations

The phase composition determined by X-Ray diffraction was carried out to identify the crystallinity of TiO_2 . Patterns of samples were obtained with a Bruker AXS D-8 diffractometer using $\text{Cu-K}\alpha$ radiation in Bragg–Brentano geometry in the 2θ range from 10 to 90. The optical properties of the samples were analyzed by UV-1600 spectrophotometer. The transmittance spectra of the TiO_2 suspensions were recorded on a UV–vis–NIR spectrophotometer Lambda 950 (Perkinelmer). The structural morphology of the prepared powders was analyzed by transmission electron microscopy (TEM) using Tecnai G² 12 TWIN, a 120 kV.

Photocatalytic Activity Measurement

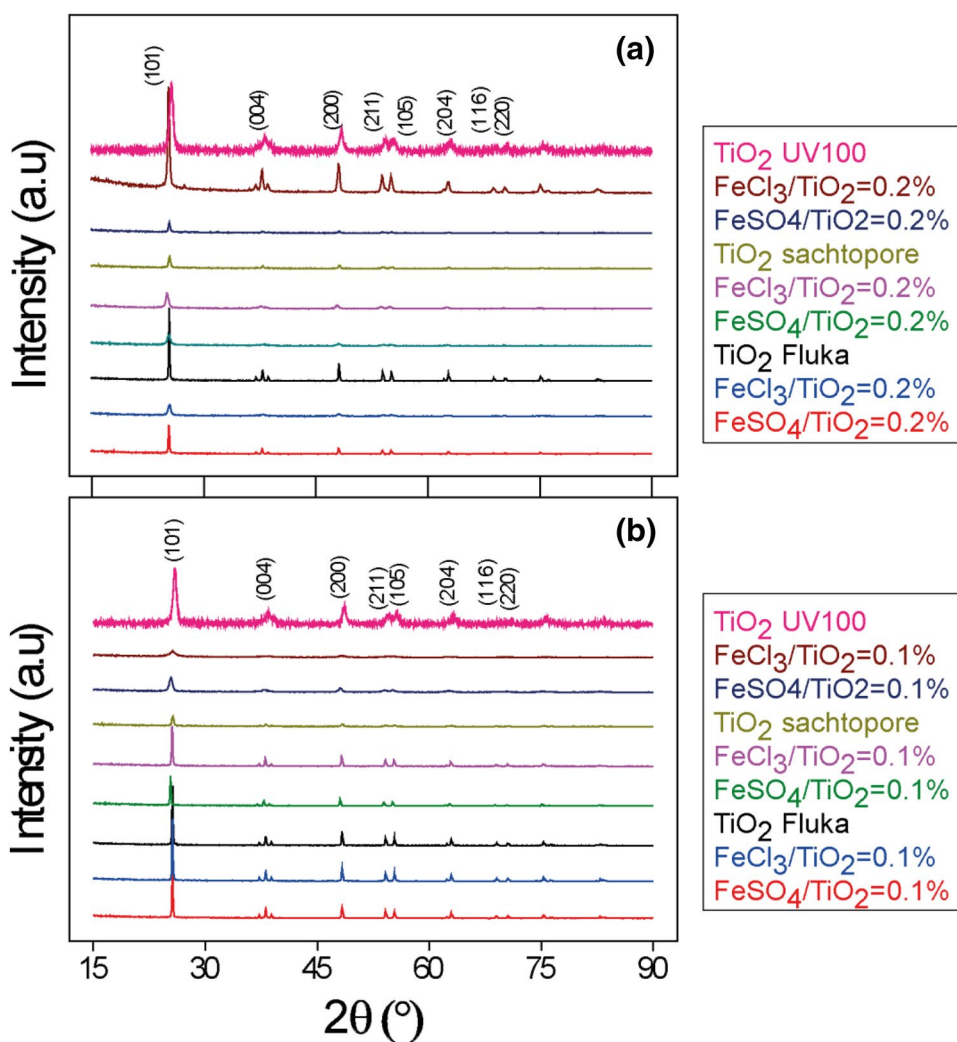
The photocatalytic process was conducted using a pyrex beaker (10 ppm of methyl orange solution and 0.5 g/L of TiO_2 photocatalyst) surrounded by a cylindrical reactor containing four vertical lamps. The instance between the light

source and the solution was between 3 and 3.5 cm. Four 15 W lamps were produced as a source of UV irradiation. The same procedure was performed to study the photocatalytic performance of all photocatalysts. The reaction mixture was magnetically stirred in dark for 45 min to establish the adsorption/desorption equilibrium. Then, at regular time intervals, 2 mL of the solution was taken out, centrifuged and filtered through 0.2 μm Millipore filter. The filtrates obtained were then analyzed by UV–vis spectrophotometer.

Results and Discussion

Iron- TiO_2 nanoparticles were synthesized with different types of TiO_2 doped with iron. X-ray diffraction (XRD) analysis was performed to assess the structure and phase purity of the samples. Figure 1a shows XRD patterns of different type of $\text{Fe/TiO}_2=0.2\%$ prepared by coprecipitation. It was observed that all the peaks are perfectly indexed to anatase TiO_2 structure (JCPDS no. 21-1272; Fig. 1a). No

Fig. 1 X-ray powder diffraction spectra of: **a** $\text{Fe/TiO}_2=0.2\%$ and **b** $\text{Fe/TiO}_2=0.1\%$



other diffraction peaks of rutile or brookite were detected. Similar patterns were observed for doped and undoped photocatalysts. The absence of characteristic peaks of iron oxides phases may indicate the high metallic dispersion (Riaz et al. 2011, 2012; Sood et al. 2015) or due to the low concentration of Fe-doping (Riaz et al. 2011). We found that there is no appearance of any difference in crystallinity between doped and undoped TiO₂. Furthermore, Fig. 1a shows the intensity of peaks that decreased by the introduction of dopant. In fact, the Scherrer equation (Eq. 1) was applied to calculate the average crystallite size of photocatalysts analyzed by XRD. In addition, the evaluation of the particle size obtained from the XRD patterns are listed in Table 1:

$$D = 0.94 \left(\frac{\lambda}{\beta} \right) \cos \theta, \quad (1)$$

where D is the crystallite size, λ is the wavelength of the X-ray radiation ($\text{CuK}\alpha = 1.5406 \text{ \AA}$), shape factor k is related to the crystallite shape, usually taken as 0.9. Moreover, the average grain sizes of the coprecipitated samples are listed in Table 1. It has been found that the amount of Fe has a small influence on the size and distribution of the

Table 1 Crystallite sizes, bandgap energies and absorption edges of photocatalysts

| | Crystallite size (nm) | Bandgap energy (eV) | Absorption edge (nm) |
|---|-----------------------|---------------------|----------------------|
| Photocatalysts | | | |
| TiO ₂ (Sachtopore) | | | |
| TiO ₂ | 32.27 | 3.22 | 385 |
| FeSO ₄ /TiO ₂ =0.2% | 32.27 | 3.18 | 389 |
| FeCl ₃ /TiO ₂ =0.2% | 32.26 | 3.18 | 389 |
| FeSO ₄ /TiO ₂ =0.1% | 42.99 | 3.19 | 388 |
| FeCl ₃ /TiO ₂ =0.1% | 43.01 | 3.19 | 388 |
| Photocatalysts | | | |
| TiO ₂ (Hombikat UV100) | | | |
| TiO ₂ | 8.81 | 3.11 | 398 |
| FeSO ₄ /TiO ₂ =0.2% | 18.44 | 3.07 | 403 |
| FeCl ₃ /TiO ₂ =0.2% | 21.5 | 2.97 | 418 |
| FeSO ₄ /TiO ₂ =0.1% | 18.43 | 3.07 | 403 |
| FeCl ₃ /TiO ₂ =0.1% | 32.26 | 3.06 | 405 |
| Photocatalysts | | | |
| TiO ₂ (Fluka) | | | |
| TiO ₂ | 43.02 | 3.17 | 391 |
| FeSO ₄ /TiO ₂ =0.2% | 21.51 | 3.04 | 407 |
| FeCl ₃ /TiO ₂ =0.2% | 25.81 | 3.11 | 398 |
| FeSO ₄ /TiO ₂ =0.1% | 43.02 | 3.15 | 393 |
| FeCl ₃ /TiO ₂ =0.1% | 43.02 | 3.17 | 391 |

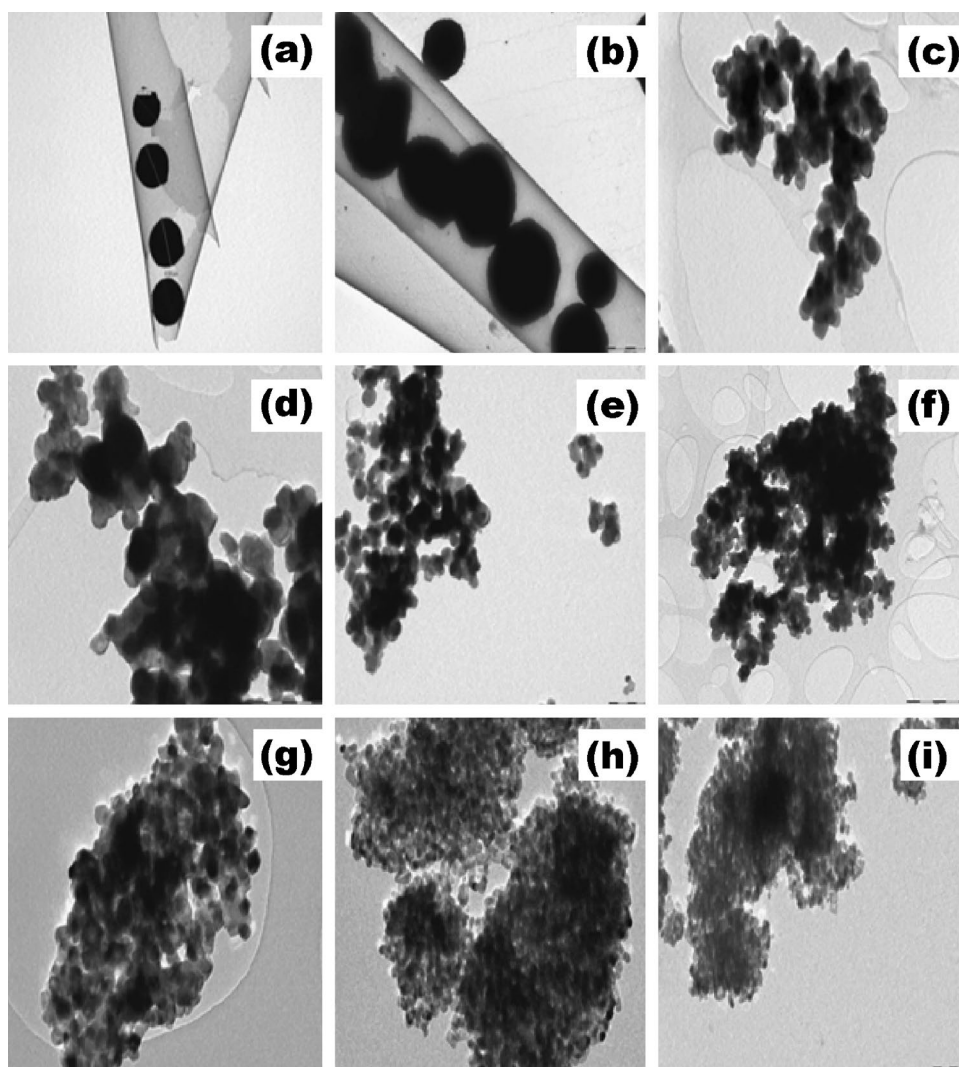
photocatalysts. The results showed that the crystallite size of the sachtopore TiO₂ and TiO₂ UV100 increases with the increase in the doping concentration. For TiO₂ fluka, the grain size increases by introducing an iron dopant unlike to TiO₂ UV 100, which could be because the metals introduced were not incorporated into the TiO₂ structure. On the other hand, in the case of TiO₂ sachtopore, the size of the crystallite does not show any significant difference in particle size, by doping with iron.

Figure 1b shows the X-ray diffraction pattern of Fe/TiO₂=0.1%. TiO₂ nanoparticles were assigned to the anatase structure and no other phases as brookite or rutile were detected. The crystallite phases corresponding to the formation of mixed compounds (Fe₂O₃ or Fe_xTiO_y) are not observed due to the low concentration of iron ions. This could be assigned to fine dispersed iron ions in small amount in most of the TiO₂ nanopowders. A slight shift in the position of the strongest peak relative to (101) was observed. This might be due to the introduction of iron, which revealed the substitution of Ti⁴⁺ by Fe³⁺ in the TiO₂ network (Jiang et al. 2015). Fe³⁺ ions are incorporated into the crystal structure of TiO₂ by substituting Ti⁴⁺ or by binding to interstitial sites (Rasoulnezhad et al. 2018). It has been observed that the intensity of the anatase decreased, which could be attributed to the deformation of the crystal lattice. In the case of sachtopore TiO₂ and TiO₂ UV100, the sizes of the crystallites increase with the increase in the concentration of dopants. By contrast, for TiO₂ Fluka, the size of the crystallites of doped and undoped materials has not changed. Consequently, any modifications in the parameters of the crystal lattice and of the electronic structures were observed. Thus, Fe³⁺ ions were not incorporated into the crystal lattice of TiO₂.

The morphologies of the as-prepared Fe/TiO₂=0.2% were carried out by transmission electron microscopy (TEM). Figure 2 shows the morphologies of undoped and doped TiO₂ nanoparticles with Fe. It can be observed that all synthesized titanium dioxide nanoparticles are spherical and have a morphology similar to that of undoped TiO₂. TEM images illustrate planar surface with aggregates particles obtained for doped TiO₂. Due to aggregation, the TiO₂ particles are indistinguishable from each other and have irregular spheres.

Optical measurements were carried out at room temperature by UV-vis spectroscopy. DRS spectra of TiO₂ doped at 0.2% and of undoped TiO₂ photocatalysts are presented in Fig. 3a. The samples were analyzed over a spectral range of 300–800 nm. The transmittance of titanium oxide nanoparticles has been shown to decrease. This decrease in the transmittance of TiO₂ powders is due to the fundamental absorption of light. All the spectra have an abruptly increasing absorption edge. The optical bandgap E_g values of TiO₂ was determined from their absorbance spectra. The

Fig. 2 TEM images of **a** TiO₂ Sachtopore, **b** FeSO₄/TiO₂=0.2%, **c** FeCl₃/TiO₂=0.2%, **d** TiO₂ Fluka, **e** FeSO₄/TiO₂=0.2%, **f** FeCl₃/TiO₂=0.2%, **g** TiO₂ Hombikat UV100, **h** FeCl₃/TiO₂=0.2% and **i** FeSO₄/TiO₂=0.2%

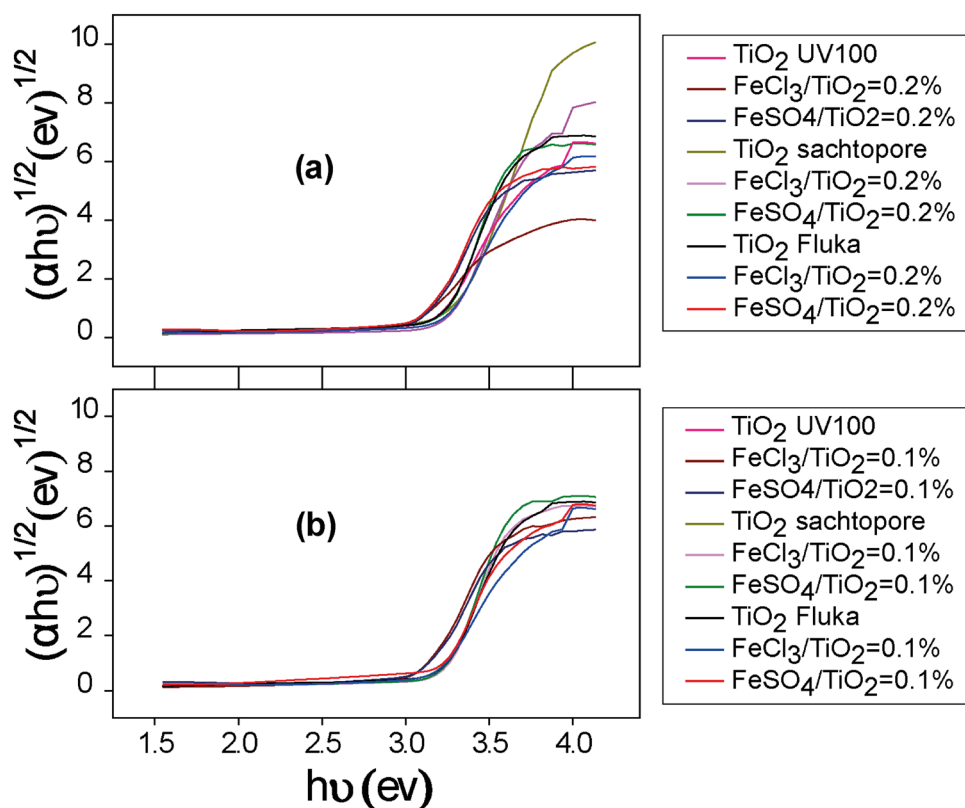


Eg values for bandgap materials were calculated from the plot $(\alpha h\nu)^{1/2}$ versus photon energy ($h\nu$) and by extrapolation of the linear portion of the curves until they intercept the photon energy axis (Fig. 3a). Fe-doped TiO₂ nanoparticles showed similar spectra compared to undoped TiO₂ with a slight shift in the absorption threshold. Moreover, no significant change was between the undoped and Fe-doped TiO₂ catalysts. On the other hand, for the different type of TiO₂, the introduction of iron does not affect the value of the gap. A significant effect of iron precursors on the energy gap has not been observed. The bandgap values of iron-doped TiO₂ powders vary from 3.22 to 2.97 eV. The DRS spectra of samples of TiO₂ doped with iron have the same absorption threshold. The values of the energy gap thus obtained are in line with previous studies using the same method and different dopants (Khan et al. 2002; Irie et al. 2003). The absorption of Fe-doped TiO₂ shift towards the beginning of the visible light zone due to the presence of iron. It has been observed that the amount of dopants (Fig. 3a) has a slight

blue shift. The bandgap energies are reported in Table 1. In the case of TiO₂ Fluka and TiO₂ UV100, the energetic gap decreases with the increase in the amount of iron ions. This could be attributed to the introduction of conduction and valence bands. On the other hand, for the other types of TiO₂, the iron content does not affect the value of the gap. Therefore, there is no significant effect of iron precursors on the energy gap for TiO₂ sachtopore. The UV–vis diffuse reflectance spectra of Fe/TiO₂=0.1% powders are shown in Fig. 3b. The spectra show a slight shift offset of the absorption edge by the introduction of iron ions. The absorption edge of TiO₂ samples was shifted towards the beginning of the visible region compared to undoped TiO₂ (Table 1). Furthermore, the absorption wavelength of the doped TiO₂ was slightly increased but does not cause a significant change.

To assess the photoactivity of the samples, we conducted methyl orange (MO) degradation experiments. MO dye was chosen as a model pollutant due to its frequent use in the textile industry. MO initial concentration used in this work

Fig. 3 Plots of $(\alpha h\nu)^{1/2}$ versus photon energy ($h\nu$) of undoped and Fe-doped TiO₂ photocatalysts: **a** Fe/TiO₂=0.2% and **b** Fe/TiO₂=0.1%



was 10 mg/L, the amount of catalysts was 0.5 g/L and the photocatalytic efficiency of the synthesized Fe-doped TiO₂ samples was followed using Eq. (2).

$$\ln\left(\frac{C}{C_0}\right) = -Kt, \quad (2)$$

where C/C_0 is the normalized MO concentration, t is the reaction time, and k is the reaction rate constant (min^{-1}). It has been observed that the degradation rate is faster in the case of TiO₂ doped with Fe than in pure nanomaterials with TiO₂. TiO₂ sachtopore samples are more effective at degrading methyl orange than the other types of TiO₂ used in current work. The photocatalytic efficiency of TiO₂ depends on the nature of the catalyst used and the concentration of dopant. The best photo-performances are explained by the fact that the recombination time of the electron/hole pairs is longer (K et al. 2014), which favors surface-trapped electrons and surface-trapped holes of the photocatalysts (Irie et al. 2003). Some authors have suggested that Fe³⁺ increases the rate of recombination, while others reported the beneficial effects of Fe³⁺ in the separation of photogenerated electrons and holes, and on the shift of the absorption range towards the visible by reducing the bandgap. Thus leading to an increase in the photocatalytic activity (K et al. 2014; Moradi et al. 2018). TiO₂ sachtopore nanoparticles exhibit higher photocatalytic activity and faster degradation

rates than TiO₂ fluka. Table 2 shows the values of the k rate constants and the half-life $t_{1/2}$ using different photocatalysts. The degradation of methyl orange follows the pseudo first-order reaction model. The photoactivity is almost identical for all Fe-doped TiO₂. The correlation coefficients calculated from the experimental data are relatively good.

The photocatalytic activities of as-synthesized Fe/TiO₂=0.1% (the mass percentage of dopant in the titanium dioxide powder) for the degradation of methyl orange are shown in Fig. 4b. We found that compared with undoped TiO₂, the prepared photocatalysts have a much higher photocatalytic efficiency than undoped TiO₂. The presence of Fe³⁺ does not modify the position of the valence and conduction band of TiO₂ (Adyani et al. 2018), but it creates new energy levels in the bandgap, between the valence and the conduction band (Kong et al. 2017). The higher photocatalytic activity of Fe-doped TiO₂ in comparison to undoped TiO₂ could be assigned to the substitution of Ti⁴⁺ ions with Fe³⁺, which acts as electron acceptors, promoting photogenerated charge separation leading to •OH radical formation on the surface of the oxide lattice (Mancuso et al. 2020; Khairy et al. 2014). The efficiencies of MO degradation for Fe-doped TiO₂=0.2% is higher than Fe-doped TiO₂=0.1% under UV irradiation for 2 h. This improvement in photocatalytic activity could be due to active surface sites and/or slower electron/hole recombination. According to Shen J H et al. work, the efficiencies of AO7 degradation over P25,

Table 2 Kinetic parameters of TiO₂ under UV irradiation

| | $K \cdot 10^{-3}$ (min ⁻¹) | $t_{1/2}$ (min) | Degradation efficiency in 2 hours (%) | R^2 |
|---|---|--------------------|--|-------|
| Photocatalysts | | | | |
| TiO₂ (Sachtopore) | | | | |
| TiO ₂ | 1.2 | 578 | 13 | 0.97 |
| FeSO ₄ /TiO ₂ =0.2% | 2.5 | 277 | 25 | 0.99 |
| FeCl ₃ /TiO ₂ =0.2% | 2 | 346 | 19 | 0.99 |
| FeSO ₄ /TiO ₂ =0.1% | 2 | 346 | 20 | 0.98 |
| FeCl ₃ /TiO ₂ =0.1% | 1.5 | 462 | 17 | 0.97 |
| Photocatalysts | | | | |
| TiO₂ (Hombikat UV100) | | | | |
| TiO ₂ | 0.8 | 866 | 9 | 0.97 |
| FeSO ₄ /TiO ₂ =0.2% | 1.6 | 433 | 17 | 0.99 |
| FeCl ₃ /TiO ₂ =0.2% | 2.3 | 301 | 24 | 0.98 |
| FeSO ₄ /TiO ₂ =0.1% | 1.3 | 533 | 15 | 0.99 |
| FeCl ₃ /TiO ₂ =0.1% | 0.9 | 770 | 11 | 0.97 |
| Photocatalysts | | | | |
| TiO₂ (Fluka) | | | | |
| TiO ₂ | 0.3 | 2310 | 5 | 0.98 |
| FeSO ₄ /TiO ₂ =0.2% | 1.5 | 462 | 17 | 0.98 |
| FeCl ₃ /TiO ₂ =0.2% | 1.4 | 495 | 15 | 0.98 |
| FeSO ₄ /TiO ₂ =0.1% | 0.4 | 1733 | 5 | 0.98 |
| FeCl ₃ /TiO ₂ =0.1% | 0.9 | 770 | 10 | 0.99 |

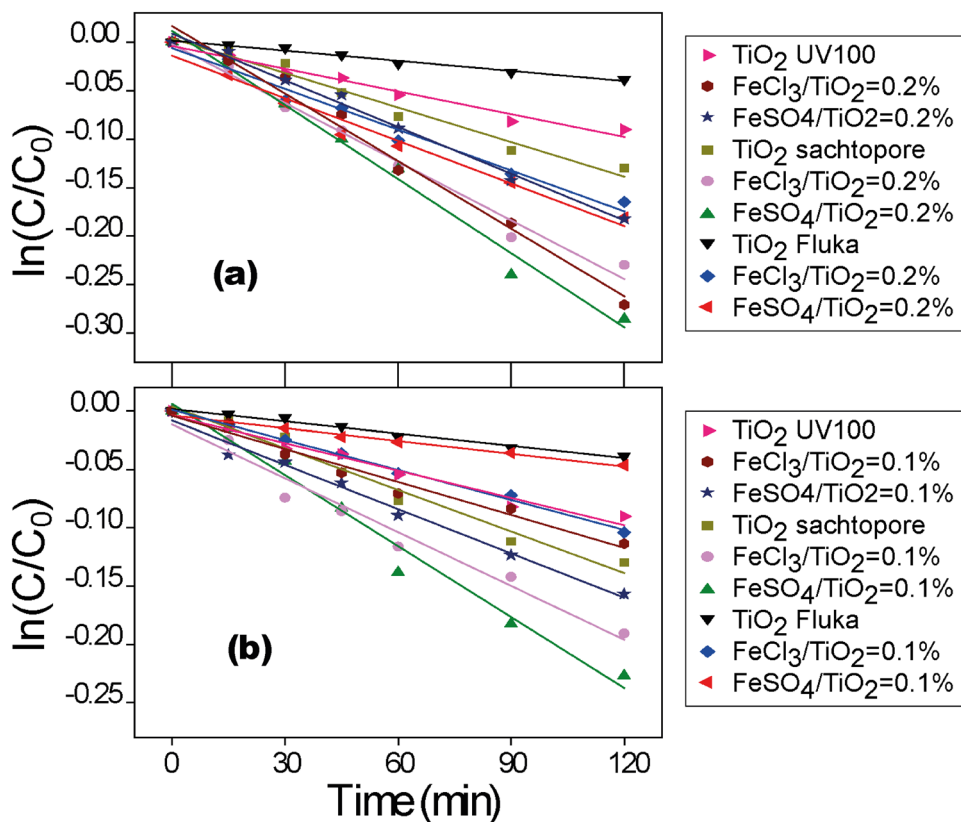
bare, and Fe-doped TiO₂ under UV irradiation for 6 h were 36%, 32% and 50%, respectively.

On the other hand, TiO₂ doped with Fe inhibits the recombination of the photogenerated electrons and holes. Fe ion with an appropriate concentration can trap photogenerated electrons. The half-life is the time required for a quantity to reduce to half its initial value. It is clearly observed that the nanoparticles of TiO₂ doped Fe present a good photocatalytic effect. The corresponding first order degradation rate constant for all doped samples is much higher than that of undoped samples for the photodegradation of MO under the same experimental conditions. The photocatalytic activities of the photocatalysts could be influenced by the different physicochemical properties, the size of the crystallites or the specific surface.

Conclusion

Fe-doped TiO₂ nanoparticles were prepared by a simple coprecipitation method. The XRD patterns did not show the presence of iron oxide phases for all samples. Optical study showed a slight decrease in the bandgap energies, leading to an increase in the wavelength of the absorption edge. The photocatalytic activity of the Fe-doped TiO₂ was assessed under UV light irradiation. The photodegradation of methyl orange follows a pseudo first-order kinetic model.

Fig. 4 Degradation of methyl orange (MO) in the presence of undoped and Fe-doped TiO₂ photocatalysts: **a** Fe/TiO₂=0.2% and **b** Fe/TiO₂=0.1%



The photocatalytic capacity indicated that the as-prepared nanoparticles exhibited improved photocatalytic activity compared with undoped TiO₂ towards the removal of methyl orange. All prepared samples are more photoactive under UV irradiation than undoped TiO₂. The photocatalytic efficiency of Fe-doped TiO₂ coprecipitated nanoparticles depend on the nature of TiO₂, the quantity of photocatalysts as well as iron components. In fact, the highest degradation rate of MO was 25% in 2 h for Fe-doped TiO₂ (sachtopor) instead of undoped TiO₂ (5%).

Compliance with Ethical Standards

Conflict of interest On behalf of all authors, the corresponding author states that there is no conflict of interest.

References

- Adyani SM, Ghorbani MA (2018) Comparative study of physicochemical and photocatalytic properties of visible light responsive Fe, Gd and P single and tri-doped TiO₂ nanomaterials. *J Rare Earth* 36(1):72–85
- Anjum M, Miandad R, Waqas M, Gehany F, Barakat MA (2016) Remediation of wastewater using various nano-materials. *Arab J Chem*. <https://doi.org/10.1016/j.arabjc.2016.10.004>
- Auta M, Hameed BH (2013) Coalesced chitosan activated carbon composite for batch and fixed-bed adsorption of cationic and anionic dye. *Coll Surf B* 105:199–206
- Bilińska L, Gmurek M, Ledakowicz S (2017) Textile wastewater treatment by AOPs for brine reuse. *Process Saf Environ Prot* 109:420–428
- Black AP, Suzuki H, Higashi M, Frontera C, Ritter C, De C, Sundaresan A, Abe R, Fuertes A (2018) New rare earth hafnium oxynitride perovskites with photocatalytic activity in water oxidation and reduction. *Chem Comm* 54:1525–1528
- Chatzisyameon E, Petrou C, Mantzavinos D (2013) Photocatalytic treatment of textile dye house effluents with simulated and natural solar light. *Global NEST J* 15:21–28
- Chnirheb A, Harir M, Kanawati B, Fekete A, El Azzouzi M, Hertkorn N, Schmitt-Kopplin Ph (2012) Efficiency and degradation products elucidation of the photodegradation of mefenpyrdiethyl in water interface using TiO₂ P-25 and Hombikat UV100. *J Environ Sci* 24:1686–1693
- Crişana M, Mardareb D, Ianculescuc A, Drăgana N, Niţoid I, Crişana D, Voicescua M, Todana L, Oancea P, Adomniţeb C, Dobromirf M, Gabrovskag M, Vasile B (2018) Iron doped TiO₂ films and their photoactivity in nitrobenzene removal from water. *Appl Surf Sci* 455:201–215
- Cruz IF, Freire C, Araújo JP, Pereira C, Pereira AM (2018) Multifunctional ferrite nanoparticles: from current trends toward the future, pp 63–116. Chapter 3: Portugal
- Ferroudj N, Nzimoto J, Davidson A, Talbot D, Briot E, Dupuis V, Abramson S (2013) Maghemite nanoparticles and maghemite/silica nanocomposite microspheres as magnetic Fenton catalysts for the removal of water pollutants. *Appl Catal B: Environ* 136:9–18
- Ghaedi M, Karimi F, Barazesh B, Sahraei R, Daneshfar A (2013) Removal of reactive orange 12 from aqueous solutions by adsorption on tin sulfide nanoparticle loaded on activated carbon. *J Ind Eng Chem* 19:756–763
- Gomathi Devi L, Kavitha R (2014) Review on modified N-TiO₂ for green energy applications under UV/visible light: selected results and reaction mechanisms. *RSC Adv* 4:28265–28299
- Han F, Kambala VSR, Srinivasan M, Rajarathnam D, Naidu R (2009) Tailored titanium dioxide photocatalysts for the degradation of organic dyes in wastewater treatment: a review. *Appl Catal A-Gen* 359:25–40
- Hejazi R, Mahjoub AR, Cheshm Khavarb AH, Khazaee Z (2020) Fabrication of novel type visible-light-driven TiO₂@MIL-100 (Fe) microspheres with high photocatalytic performance for removal of organic pollutants. *J Photochem Photobiol A: Chem* 400:112644
- Irie H, Watanabe Y, Hashimoto K (2003) Carbon-doped anatase TiO₂ powders as a visible-light sensitive photocatalyst. *Chem Lett* 32:772–773
- Jiang X, Wang F, Li G, Qi L, Liu P, Ding Y, Zhang S, Yang M (2015) Low temperature synthesis and mechanism of finely dispersed nanorod rutile titanium dioxide. *RSC Adv* 5:62160–62166
- Khairy M, Zakaria W (2014) Effect of metal-doping of TiO₂ nanoparticles on their photocatalytic activities toward removal of organic dyes. *Egypt J Pet* 23:419–426
- Khan SUM, Al-Shahry M, Ingler WB (2002) Efficient photochemical water splitting by a chemically modified n-TiO₂. *Sci* 297:2243–2245
- Kong L, Wang C, Wan F, Zheng H, Zhang X (2017) Synergistic effect of surface self-doping and Fe species-grafting for enhanced photocatalytic activity of TiO₂ under visible-light. *Appl Surf Sci* 396:26–35
- Koupaie EH, Moghaddam MRA, Hashemi SH (2013) Successful treatment of high azo dye concentration wastewater using combined anaerobic/aerobic granular activated carbon-sequencing batch biofilm reactor (GAC-SBBR): simultaneous adsorption and biodegradation processes. *Water Sci Technol* 67:1816–1821
- Liao Y, Wang X, Ma Y, Li J, Wen T, Jia L, Zhong Z, Wang L, Zhang D (2016) New mechanistic insight of low temperature crystallization of anodic TiO₂ nanotube array in water. *Cryst Grow Desig* 16(4):1786–1791
- Liu Y, Chen X (2017) Black titanium dioxide for photocatalysis. *Semiconduct Semimet* 97:393–428
- Mancuso A, Sacco O, Sannino D, Pragliola S, Vaiano V (2020) Enhanced visible-light-driven photodegradation of Acid Orange 7 azo dye in aqueous solution using Fe-N co-doped TiO₂. *Arab J Chem*. <https://doi.org/10.1016/j.arabjc.2020.05.019>
- Meek ME (2017) AOPs in hazard characterization for human health. *Curr Opin Toxicol* 3:80–86
- Moradi V, Jun MBG, Blackburn A, Herring RA (2018) Significant improvement in visible light photocatalytic activity of Fe doped TiO₂ using an acid treatment process. *Appl Surf Sci* 427(B):791–799
- Naira RG, Mazumdar S, Modak B, Bapatb R, Ayyub P, Bhattacharyya K (2017) The role of surface O-vacancies in the photocatalytic oxidation of Methylene Blue by Zn-doped TiO₂: a mechanistic approach. *J Photochem Photobiol A* 345(1):36–53
- Nawaz M, Sliman Y, Ercan I, Lima-Tenório MK, Tenório-Neto ET, Kaewsaneha C, Elaissari A (2019) Magnetic and pH-responsive magnetic nanocarriers, Thailand pp 41–85 Chapter 2.
- Ozawa K, Emori M, Yamamoto S, Yukawa R, Yamamoto S, Hobaru R, Fujikawa K, Sakama H, Matsuda I (2014) Electron-hole recombination time at TiO₂ single-crystal surfaces: influence of surface band bending. *J Phys Chem Lett* 5(11):1953–1957
- Pang YL, Abdullah AZ (2013) Fe³⁺ doped TiO₂ nanotubes for combined adsorption-sonocatalytic degradation of real textile wastewater. *Appl Catal B* 129:473–481
- Rasoulnezhad H, Hosseinzadeh G, Yekrang J (2018) Preparation and characterization of nanostructured S and Fe co-doped TiO₂ thin film by ultrasonic-assisted spray pyrolysis method. *J Nanostruct* 8(3):251–258

- Riaz N, Chong F, Dutta BK, Man ZB, Khan MS, Nurlaela E (2011) Effect of calcination temperature on Orange II photocatalytic degradation using Cu: Ni/TiO₂ under visible light. Third National Postgraduate Conference (NPC), IEEE: University Teknologi PETRONAS (UTP), Tronoh, Malaysia 1–5.
- Riaz N, Chong FK, Dutta BK, Man ZB, Khan MS, Ramli RM (2012) Azo dye degradation using Cu/TiO₂ under visible light: effect of metal loading. 2nd International Conference on Process Engineering and Advanced Materials (ICPEAM), IEEE: Kuala Lumpur 6.
- Shen JH, Chuang HY, Jiang ZW, Liu XZ, Horng JL (2020) Novel quantification of formation trend and reaction efficiency of hydroxyl radicals for investigating photocatalytic mechanism of Fe-doped TiO₂ during UV and visible light-induced degradation of acid orange 7. *Chemosphere* 251:126380
- Sood S, Umar A, Mehta SK, Kumar Kansal SK (2015) Highly effective Fe-doped TiO₂ nanoparticles photocatalysts for visiblelight driven photocatalytic degradation of toxic organic compounds. *J Colloid Interface Sci* 450:213–223
- Srikanth B, Gouthama R, Badri Narayana R, Ramprasatha A, GopinathK P, Sankaranarayanan AR (2017) Recent advancements in supporting materials for immobilised photocatalytic applications in waste water treatment. *J Environ Manag* 200:60–78
- Sun L, Guan J, Xu Q, Yang X, Wang J, Hu X (2018) Synthesis and applications of molecularly imprinted polymers modified TiO₂ nanomaterials: a review. *Polymers* 10(11):1248
- Taghizadeh F, Ghaedi M, Kamali K, Sharifpour E, Sahraie R, Purkait MK (2013) Comparison of nickel and/or zinc selenide nanoparticle loaded on activated carbon as efficient adsorbents for kinetic and equilibrium study of removal of Arsenazo (III) dye. *Powder Techn* 245:217–226
- Weng XL, Zeng QS, Zhang YL, Dong F, Wu ZB (2016) Facile approach for the syntheses of ultrafine TiO₂ nanocrystallites with defects and C heterojunction for photocatalytic water splitting. *ACS Sustain Chem Eng* 4:4314–4320
- Wu W, Jiang C, Roy VAL (2016) Designed synthesis and surface engineering strategies of magnetic iron oxide nanoparticles for biomedical application. *Nanoscale* 8:19421–19474
- Yanga G, Yanb Z, Xiao T (2012) Preparation and characterization of SnO₂/ZnO/TiO₂ composite semiconductor with enhanced photocatalytic activity. *Appl Surf Sci* 258:8704–8712
- Yan-Xia H, Chuan-Lu Y, Mei-Shan W, Xiao-Guang M, Li-Zhi W (2015) Enhancing the visible-light absorption of TiO₂ with the use of key N Co, and Na dopant concentrations. *Sol Energ Mat Sol* 132:94–100
- Zahid R, Manzoor M, Rafq A, Ikram M, Nafees M, Butt AR, Hussain SG, Ali S (2018) Influence of iron doping on structural, optical and magnetic properties of TiO₂ nanoparticles. *Elect Mater Lett* 14:587–593
- Zhang DQ, Eng CY, Stuckey DC, Zhou Y (2017a) Effects of ZnO nanoparticle exposure on wastewater treatment and soluble microbial products (SMPs) in an anoxic-aerobic membrane bioreactor. *Chemosphere* 171:446–459
- Zhang W, Yin JR, Tang XQ, Zhang P, Ding YH (2017b) Density functional theory studies on the structural and physical properties of Cu-doped anatase TiO₂ (101) surface. *Physica E* 85:259–263